Lili Wang
e-mail: wllxxx@yahoo.com.cn
State Key Laboratory of Nonlinear Mechanics (LNM),
Institute of Mechanics, Chinese Academy of Sciences; Beijing, P.R. China
Institute of Applied Physics and Computational Mathematics, Beijing, P. R. China

Jinghui Zhang

Chao Wang

Shiyue Hu

Civil College,
Xi'an Jiaotong University,
Xi'an, P.R. China

Identification of Nonlinear Systems Through Time-frequency Filtering Technique

In the previous paper, a class of nonlinear system is mapped to a so-called skeleton linear model (SLM) based on the joint time-frequency analysis method. Behavior of the nonlinear system may be indicated quantitatively by the variance of the coefficients of SLM versus its response. Using this model we propose an identification method for nonlinear systems based on nonstationary vibration data in this paper. The key technique in the identification procedure is a time-frequency filtering method by which solution of the SLM is extracted from the response data of the corresponding nonlinear system. Two time-frequency filtering methods are discussed here. One is based on the quadratic time-frequency distribution and its inverse transform, the other is based on the quadratic time-frequency distribution and the wavelet transform. Both numerical examples and an experimental application are given to illustrate the validity of the technique.
[DOI: 10.1115/1.1545769]

1 Introduction

The dynamic behavior of a nonlinear system generally varies with the instantaneous response. In our previous paper [1] of this work, based on the joint time-frequency analysis [2], a time-frequency masking operator together with the effective time-frequency region of the asymptotic signal is defined. Under these mathematical foundations, we deduced a time-varying linear system, that is, the skeleton linear model (SLM), for a class of nonlinear system. The dynamic behavior of SLM is similar to that of the nonlinear system. For the following nonlinear system

$$m\ddot{y}+F(y,\dot{y})=u \tag{1}$$

the corresponding SLM is

$$\ddot{x}+2h_0\dot{x}+\omega_0^2 x=\frac{1}{m}u \tag{2}$$

$$\omega_0^2=\frac{1}{\pi ma}\int_0^{2\pi}F(a\cos\varphi,-a\omega\sin\varphi)\cos\varphi d\varphi \tag{3}$$

$$h_0=-\frac{1}{2\pi ma\omega}\int_0^{2\pi}F(a\cos\varphi,-a\omega\sin\varphi)\sin\varphi d\varphi \tag{4}$$

where ω_0 and h_0 denotes the instantaneous undamped natural frequency and the instantaneous decay coefficient, respectively. They are all variables varying slowly with time.

The response of SLM (2) is the principal component of that of the corresponding nonlinear system (1). And we call the regressive curves, $\omega_0(a,\omega)$ and $h_0(a,\omega)$, *the frequency skeleton curve and the damping skeleton curve*, respectively. They indicate the main nonlinear behavior of the system in visual forms concisely.

In this paper we discuss the identification procedure of the skeleton curves based on the vibration data of the nonlinear system (1). The reader is referred to Ref. [1] for necessary background knowledge and details.

2 Identification of the Skeleton Curves

2.1 Choice of the Excitation Signal. The relationship between LSM and the nonlinear system, expressed by Eqs. (3) and (4), is only deduced under certain conditions. It is true when an asymptotic signal takes the dominant status in $y(t)$ and its derivatives for $u(t)=0$. The relationship is also valid when the instantaneous frequency of the principal components in $y(t)$ and its derivatives approximate to that of $u(t)$ for an asymptotic excitation signal. We should choose an appropriate excitation signal to guarantee that Eqs. (3) and (4) hold true. We may use an impact signal with appropriate amplitude. The impact test is very convenient. But the precision may be poor for systems with very large damping in which there is a lack of available testing data due to the quick decay. In this instance the forced response should be adopted. To guarantee that the harmonic component is dominant in the response, the instantaneous frequency of the excitation should approximate the resonance frequency of the system. Besides, the resonance response signal may take large amplitude even with small energy excitation. A priori knowledge about the system is needed for the identification when the forced vibration testing is used.

2.2 Extracting the Response Signal of SLM from that of the Nonlinear System. Because the asymptotic signal $x(t)$ is dominant in $y(t)$, Ω_x can be estimated using the modulus of $\rho_y(t,\omega)$. $|\rho_y(t,\omega)|$ takes the maximum valve at $\omega(t)$ at any given time t. Setting a threshold value α, $0<\alpha<1$, we can take the maximum zonal with midline $\omega(t)$ which satisfies

$$|\rho_y(t,\omega)|\geq\alpha|\rho_y(t,\omega(t))| \tag{5}$$

as the estimation of Ω_x.

Then $x(t)$ can be extracted from $y(t)$ using the time-frequency masking operator on Ω_x. Because

$$x(t)\approx M(y(t),\Omega_x) \tag{6}$$

where $M(\cdot,\cdot)$ denotes the time-frequency masking operator defined in reference [1]. there is

$$\rho_x(t,\omega)=\begin{cases}\rho_y(t,\omega) & (t,\omega)\in\Omega_x\\ 0 & (t,\omega)\notin\Omega_x\end{cases} \tag{7}$$

Taking the inverse transform of $\rho_x(t,\omega)$, one yield

$$x(\tau)=\frac{1}{2\pi\cdot x^*(0)}\int\int\int\frac{\rho_x(t,\omega)}{\phi(\theta,\tau)}e^{jt\omega+j\theta(t-\tau/2)}dtd\omega d\theta \tag{8}$$

where $\phi(\theta,\tau)$ is the kernel of the quadratic time-frequency distribution of Cohen class [2].

Contributed by the Technical Committee on Vibration and Sound for publication in the JOURNAL OF VIBRATION AND ACOUSTICS. Manuscript received Sept. 2000; Revised Sept. 2002. Associate Editor: A. Vakakis.

The computation effort and storage requirement are quite large in the above method. Besides, there is singularity in Eq. (8). In section 3, a more practical time-frequency filtering technique based on the wavelet transformation is proposed.

2.3 Calculation of the Instantaneous Coefficients of SLM SLM is a special time-varying linear system with coefficients varying slowly with time. The instantaneous coefficients may be expressed by analytical functions of its instantaneous response. Calculation of the instantaneous coefficients based on the excitation signal and response signal in cases of free vibration and forced vibration are discussed in detail in references [3], [4]. For a SLM excited by an asymptotic signal and with the harmonic component be dominant in its response signal

$$\ddot{x}(t)+2h_0(t)\dot{x}(t)+\omega_0^2(t)x(t)=\frac{1}{m}u(t) \tag{9}$$

the instantaneous coefficients may be calculated as follows

$$\omega_0^2(t)=\omega^2(t)+\frac{\alpha(t)}{m}-\frac{\beta(t)\dot{a}(t)}{ma(t)\omega(t)}-\frac{\ddot{a}(t)}{a(t)}+2\frac{\dot{a}^2(t)}{a^2(t)}+\frac{\dot{a}(t)\dot{\omega}(t)}{a(t)\omega(t)} \tag{10}$$

$$h_0(t)=\frac{\beta(t)}{2m\omega(t)}-\frac{\dot{a}(t)}{a(t)}-\frac{\dot{\omega}(t)}{2\omega(t)} \tag{11}$$

where

$$a(t)=\sqrt{x^2(t)+\tilde{x}^2(t)} \tag{12}$$

$$\omega(t)=\frac{x(t)\dot{\tilde{x}}(t)-\tilde{x}(t)\dot{x}(t)}{x^2(t)+\tilde{x}^2(t)} \tag{13}$$

$$\alpha(t)=\frac{x(t)u(t)+\tilde{x}(t)\tilde{u}(t)}{x^2(t)+\tilde{x}^2(t)} \tag{14}$$

$$\beta(t)=\frac{x(t)\tilde{u}(t)-\tilde{x}(t)u(t)}{x^2(t)+\tilde{x}^2(t)} \tag{15}$$

$\tilde{u}(t)$ and $\tilde{x}(t)$ are the Hilbert transform of $u(t)$ and $x(t)$, respectively. That is

$$\tilde{u}(t)=\frac{1}{\pi}pv\int_{-\infty}^{+\infty}\frac{u(\tau)}{t-\tau}d\tau \tag{16}$$

$$\tilde{x}(t)=\frac{1}{\pi}pv\int_{-\infty}^{+\infty}\frac{x(\tau)}{t-\tau}d\tau \tag{17}$$

Where pv indicates the Cauchy principal value of the integral.

When the free vibration response date is used, Eqs. (10), (11) becomes

$$\omega_0^2(t)=\omega^2(t)-\frac{\ddot{a}(t)}{a(t)}+2\frac{\dot{a}^2(t)}{a^2(t)}+\frac{\dot{a}(t)\dot{\omega}(t)}{a(t)\omega(t)} \tag{18}$$

$$h_0(t)=-\frac{\dot{a}(t)}{a(t)}-\frac{\dot{\omega}(t)}{2\omega(t)} \tag{19}$$

The skeleton curves may be plotted directly once the instantaneous response and instantaneous coefficients of the SLM are calculated.

3 Time-Frequency Filtering Algorithm

Obviously, to extract $x(t)$ from $y(t)$, a time-vary narrow band filtering process should be used. The instantaneous central frequency of the filter ought to be set at the instantaneous frequency of $x(t)$, while its instantaneous bandwidth takes the value not less than that of $x(t)$. And the window function should be localized in both time and frequency domain. In section 2.2, the extracting is based on the quadratic time-frequency distribution and the time-frequency masking operator. But there is difficulty in calculation. In this section a more practical technique based on the wavelet transform is used.

3.1 Wavelet Transform Along the Wavelet Ridge. For the sake of completeness and better understanding, the necessary background knowledge is introduced firstly. For more details, the reader is referred to reference [5].

i) An analytic wavelet is called the asymptotic analytic wavelet if

$$\tilde{\psi}(t)=A_\psi(t)\exp(i\varphi_\psi(t)) \tag{20}$$

where

$$\left|\frac{d\varphi_\psi(t)}{dt}\right|\gg\left|\frac{1}{A_\psi(t)}\right|\cdot\left|\frac{dA_\psi(t)}{dt}\right| \tag{21}$$

Assuming that $Z(t)$ is an asymptotic signal

$$Z(t)=A(t)\exp(i\varphi(t)) \tag{22}$$

Taking the wavelet transform of $Z(t)$ with an asymptotic analyzing wavelet as the mother wavelet, yields

$$(W_{\tilde{\psi}}Z)(a,b)=\frac{1}{\sqrt{a}}\int_R Z(t)\overline{\tilde{\psi}\left(\frac{t-b}{a}\right)}dt$$

$$=\frac{1}{\sqrt{a}}\int_R\hat{A}_{a,b}(t)\exp(i\Phi_{a,b}(t))dt \tag{23}$$

where

$$\hat{A}_{a,b}(t)=A(t)A_\psi\left(\frac{t-b}{a}\right) \tag{24}$$

$$\Phi_{a,b}(t)=\varphi(t)-\varphi_\psi\left(\frac{t-b}{a}\right) \tag{25}$$

Denote the stationary point of the argument $\Phi_{a,b}(t)$ by t_s, that is

$$\dot{\Phi}_{a,b}(t_s)=0,\quad \ddot{\Phi}_{a,b}(t_s)\neq 0 \tag{26}$$

one has

$$\dot{\varphi}(t_s)=\frac{1}{a}\dot{\varphi}_\psi\left(\frac{t_s-b}{a}\right) \tag{27}$$

The *wavelet ridge*, denoted by $a_r(b)$, is defined to be the set of points (a,b) such that

$$t_s(a,b)=b \tag{28}$$

And the *wavelet curve*, denoted by $a_c(b)$, is the curve which passes through the point $(a_r(b_0),b_0)$ and satisfies

$$t_s(a,b)=b_0 \tag{29}$$

As $Z(t)$ and $\tilde{\psi}((t-b)/a)$ are both asymptotic signals, Eq. (23) represents a rapidly oscillating integral. The positive or negative parts counteract each other at most regions except the neighborhood of $t_s(a,b)$. According to the theory of asymptotic expansion it is known that if there exists only one stationary point $t_s(a,b)$ at every point in the phase plane, the first order approximation to (23) is of the form

$$(W_{\tilde{\psi}}Z)(a,b)\approx\sqrt{\frac{\pi}{2}}\frac{e^{i\pi/4\,\mathrm{sgn}(\ddot{\Phi}_{a,b}(t_s))}}{a\sqrt{|\ddot{\Phi}_{a,b}(t_s)|}}Z(t_s)\overline{\tilde{\psi}\left(\frac{t_s-b}{a}\right)} \tag{30}$$

When (a,b) is along the wavelet ridge, yields

$$(W_{\tilde{\psi}}Z)(a_r(b),b)\approx\sqrt{\frac{\pi}{2}}\frac{e^{i\pi/4\,\mathrm{sgn}(\ddot{\Phi}_{a_r(b),b}(t_s))}}{a_r(b)\sqrt{|\ddot{\Phi}_{a_r(b),b}(t_s)|}}\overline{\tilde{\psi}(0)}\cdot Z(b) \tag{31}$$

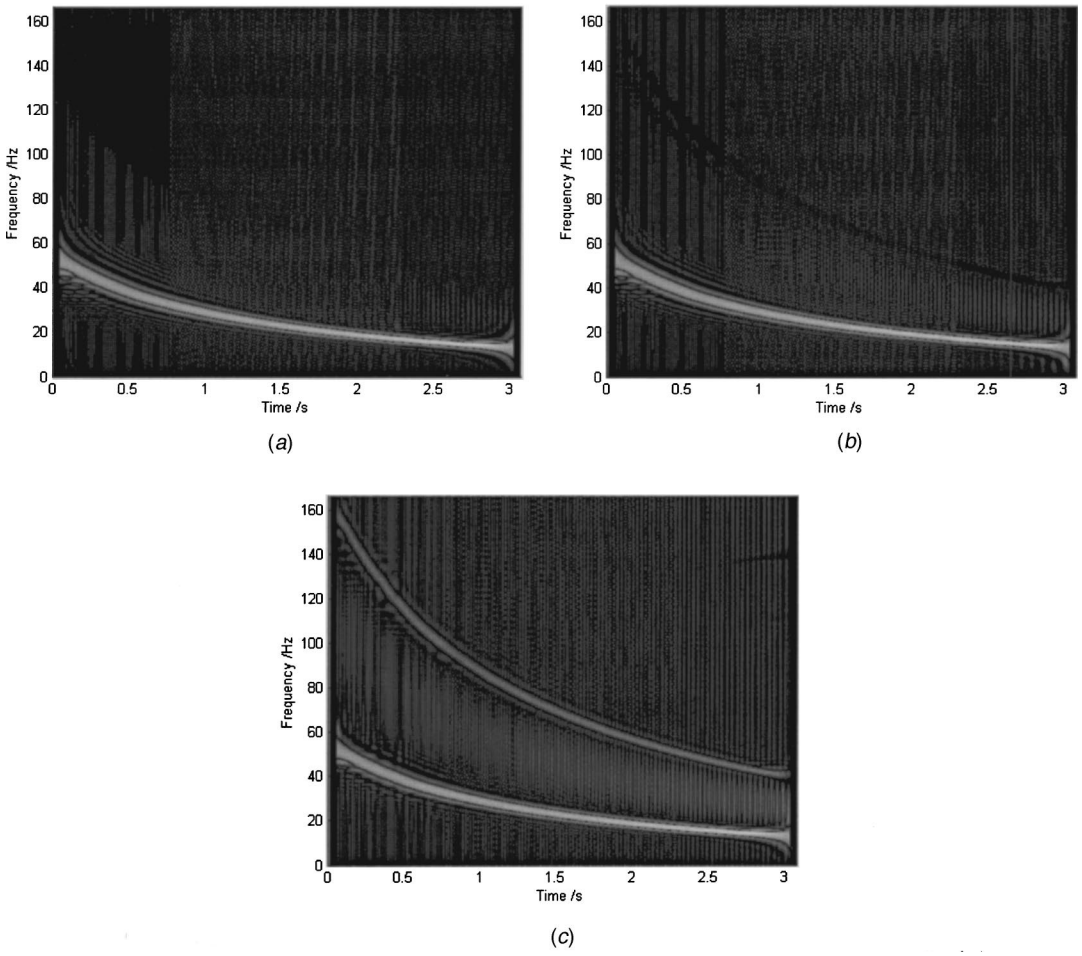

Fig. 1 Grayscale view of the modulus of quadratic time-frequency distribution (in dB) (a) $\rho_{y(t)/a_{y(t)}}$ (b) $\rho_{\dot{y}(t)/a_{\dot{y}(t)}}$ (c) $\rho_{\ddot{y}(t)/a_{\ddot{y}(t)}}$

and when (a,b) is along the wavelet curve, there is

$$(W_{\tilde{\psi}}Z)(a_c(b),b)\approx\sqrt{\frac{\pi}{2}}\frac{e^{i\pi/4\ \mathrm{sgn}(\ddot{\Phi}_{a_c,b}(b_0))}}{a_c(b)\sqrt{|\ddot{\Phi}_{a_c,b}(b_0)|}}Z(b_0)\cdot\overline{\tilde{\psi}\left(\frac{b_0-b}{a_c}\right)} \tag{32}$$

The above statements show that the value of $(W_{\tilde{\psi}}Z)(a,b)$ is determined only by $Z(\cdot)$ when (a,b) is along the wavelet ridge, and it is determined only by $\tilde{\psi}(\cdot)$ when (a,b) is along the wavelet curve.

3.2 Time-Frequency Filtering Algorithm Based on the Wavelet Transform. In this section we extract $x(t)$ from $y(t)$ through an algorithm based on the wavelet transform of $y(t)$ along the wavelet ridge of $x(t)$.

In general, $y(t)$ consists of several asymptotic signals. And usually there is no overlap for each two of them.

$$\begin{aligned} y(t)&=x(t)+Z_1(t)+Z_2(t)+\cdots\\ &=A(t)e^{j\varphi(t)}+A_1(t)e^{j\varphi_1(t)}+A_2(t)e^{j\varphi_2(t)}+\cdots \end{aligned} \tag{33}$$

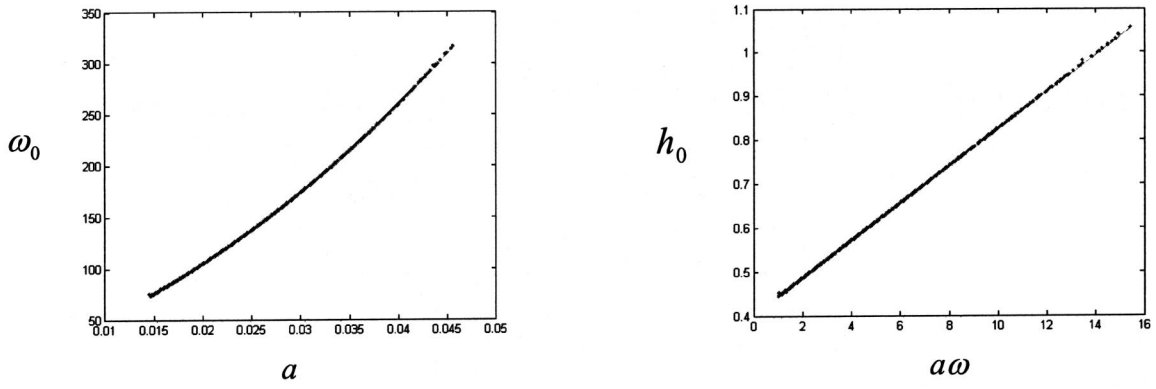

Fig. 2 The frequency and damping skeleton curves of example 1 (identified result: dot; theoretical value: line)

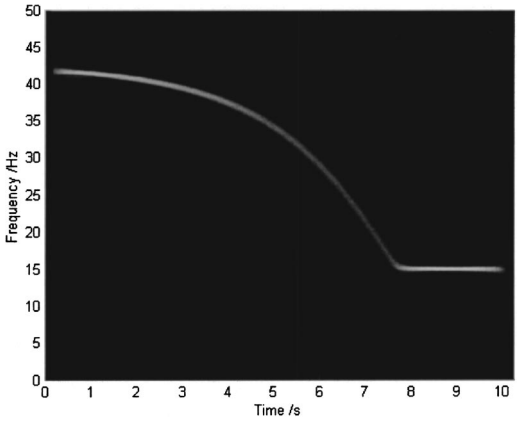

Fig. 3 Grayscale view of the modulus of $\rho_{y(t)/a_y(t)}$

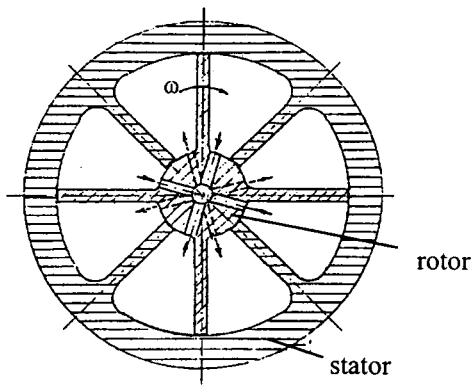

Fig. 5 Cross-section of the damper

For a given analyzing wavelet, the wavelet ridge for each component is not the same. Denote the wavelet ridge of $x(t)$ by $a_r(b)$. The instantaneous frequency of $x(t)$, $\omega(t)$, can be calculated using $\rho_y(\omega,t)$. The modulus of $\rho_y(\omega,t)$ reaches the maximum value at $\omega=\omega(t)$ at any given time t

$$|\rho_y(\omega(t),t)|=\max \tag{34}$$

Then the wavelet ridge of $x(t)$ is calculated

$$a_r(b)=\frac{\dot{\varphi}_{\psi}(0)}{\omega(b)} \tag{35}$$

For example, taking the Morlet wavelet [6] as the analyzing wavelet, its mother wavelet is

$$\tilde{\psi}(t)=e^{-t^2/2}e^{i\omega_0 t} \tag{36}$$

so one has

$$a_r(b)=\frac{\omega_0}{\omega(b)} \tag{37}$$

Furthermore, an iterative algorithm is given in reference [5] using the nature of the wavelet curve.

To obtain $x(t)$, taking the wavelet transform of $y(t)$ along the wavelet ridge of $x(t)$

$$\begin{aligned}
&W_{\tilde{\psi}}y(t)(a_r(b),b)\\
&\quad=W_{\tilde{\psi}}x(t)(a_r(b),b)+\sum_{j=1}^{\infty}W_{\tilde{\psi}}Z_j(t)(a_r(b),b)\\
&\quad=\frac{1}{\sqrt{a_r(b)}}\int_R x(t)\tilde{\psi}\left(\frac{t-b}{a_r(b)}\right)dt\\
&\qquad+\sum_{j=1}^{\infty}\frac{1}{\sqrt{a_r(b)}}\int_R Z_j(t)\tilde{\psi}\left(\frac{t-b}{a_r(b)}\right)dt\\
&\quad\approx\sqrt{\frac{\pi}{2}}\frac{e^{i\pi/4\ \mathrm{sgn}(\ddot{\Phi}_{a_r(b)}(t_s))}}{a_r(b)\sqrt{|\ddot{\Phi}_{a_r(b)}(t_s)|}}x(t_s)\overline{\tilde{\psi}\left(\frac{t_s-b}{a_r(b)}\right)}\\
&\qquad+\sum_{j=1}^{\infty}\sqrt{\frac{\pi}{2}}\frac{e^{i\pi/4\ \mathrm{sgn}(\ddot{\Phi}_{a_r^i(b)}(t_s^j))}}{a_r^i(b)\sqrt{|\ddot{\Phi}_{a_r^i(b)}(t_s^j)|}}Z_j(t_s^j)\overline{\tilde{\psi}\left(\frac{t_s^j-b}{a_r^i(b)}\right)}
\end{aligned} \tag{38}$$

where t_s denotes the stationary point of $x(t)$ with respect to the point $(a_r(b),b)$ in the phase plane, and t_s^j is that of $Z_j(t)$.

$$t_s^j\neq t_s=b \tag{39}$$

As a function with compact support, $\tilde{\psi}(t)$ reaches the maximum value at $t=0$, and decays to zero quickly as $|t|$ increases. The following equation yields as long as the instantaneous frequency of the other components is not close to that of $x(t)$.

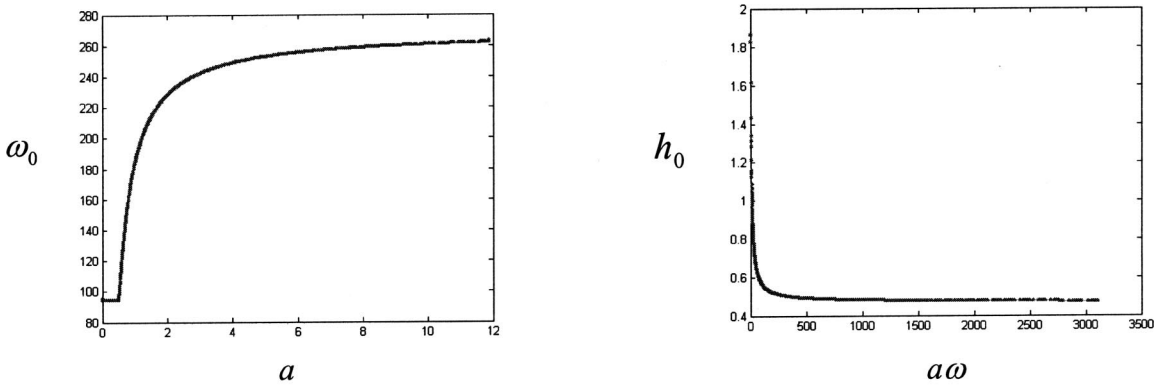

Fig. 4 The frequency and damping skeleton curves of example 2 (identified result: dot; theoretical value: line)

Table 1

l (m)	J (kg·m^2)	M (kg)	l_1 (m)	l_2 (m)	K (N/m)
0.65	0.35	3.25	0.19	0.39	6840

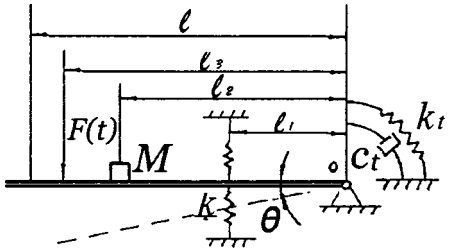

Fig. 6 The testing system

$$\tilde{\psi}\left(\frac{t_s^j-b}{a}\right)\approx 0 \tag{40}$$

thus

$$W_\psi y(t)(a_r(b),b)\approx \sqrt{\frac{\pi}{2}}\frac{e^{i\pi/4\ \mathrm{sgn}(\ddot{\Phi}_{a_r(b)}(t_s))}}{a_r(b)\sqrt{|\ddot{\Phi}_{a_r(b),b}(t_s)|}}\overline{\tilde{\psi}(0)}\cdot x(b) \tag{41}$$

where

$$\ddot{\Phi}_{a_r(b),b}(t_s)=-\frac{1}{[a_r(b)]^2}[\dot{a}_r(b)\dot{\varphi}_\psi(0)+\ddot{\varphi}_\psi(0)] \tag{42}$$

So x can be calculated through the wavelet transform of y along the wavelet ridge of x

$$x(b)=\sqrt{\frac{\pi}{2}}\sqrt{|\dot{a}_r(b)\dot{\varphi}_\psi(0)+\ddot{\varphi}_\psi(0)|}\cdot\frac{W_\psi y(t)(a_r(b),b)}{A_\psi(0)}\cdot e^{-i\pi/4\ \mathrm{sgn}\{-\dot{a}_r(b)\dot{\varphi}_\psi(0)+\ddot{\varphi}_\psi(0)/[a_r(b)]^2\}} \tag{43}$$

The preceding result can be explained as follows: The wavelet function is localized in both time domain and frequency domain. As $\tilde{\psi}(t-b/a_r(b))$ is located at b in the time domain, and at $\dot{\varphi}_\psi(0)/a_r(b)=\dot{\varphi}(b)=\omega(b)$ in the frequency domain, it acts as a time-frequency filter. Its instantaneous central frequency is $\omega(b)$, which is the instantaneous frequency of $x(t)$. And its instantaneous pass-band equals the effective time-frequency region of $x(t)$. So all the other components besides $x(t)$ in $y(t)$ are filtered out after the filtering procedure. Obviously, most noise is also filtered out in the meantime.

4 Examples

We use two numerical examples to verify the technique developed in this paper. The fourth order Runge-Kutta arithmetic is adopted in the numerical simulation. Then the identification technique is used to study the dynamic characteristic of a torsion damper.

Example 1. Consider the following system

$$\ddot{y}+c_1\dot{y}+c_2|\dot{y}|\dot{y}+k_1y+k_2y^3+k_3y^5=0 \tag{44}$$

where

$$k_1=\pi^2,\quad k_2=3\times10^6\pi^2,\quad k_3=2\times10^9\pi^2,$$
$$c_1=0.8,\quad c_2=0.1$$

This is a polynomial system with hard spring, viscous friction and square friction. The skeleton curves are

$$\omega_0(a)=\left[k_1+\frac{3}{4}k_2a^2+\frac{5}{8}k_3a^4\right]^{1/2} \tag{45}$$

$$h_0(a\omega)=\frac{c_1}{2}+\frac{4}{3\pi}c_2a\omega \tag{46}$$

The identification is based on the free vibration data with the following initial condition.

$$y(0)=0.05,\quad \dot{y}(0)=0,\quad \ddot{y}(0)=0$$

Modulus of the quadratic time-frequency distribution of the displacement, velocity and acceleration are plotted in Fig. 1. For the sake of clarity, the signals are normalized by their instantaneous amplitudes. It is seen that the displacement signal and velocity signal are almost perfect asymptotic signals in which the harmonic components cannot be found. But in the acceleration signal, the third order harmonic component is too significant to be neglected. In this example, the instantaneous frequency of the principal component varies from 15 Hz to 54 Hz, while that of the third-order harmonic component varies from 45 Hz to 162 Hz. The skeleton curves identified together with theoretical values are shown in Fig. 2.

In this example the advantage of the time-frequency filtering technique is revealed. Because the frequency range of the principle component and the harmonic component overlap, the two components are not parted completely in the Fourier spectrum. Thus the principal component could not be extracted accurately from the response signal by using the narrow-band filtering tech-

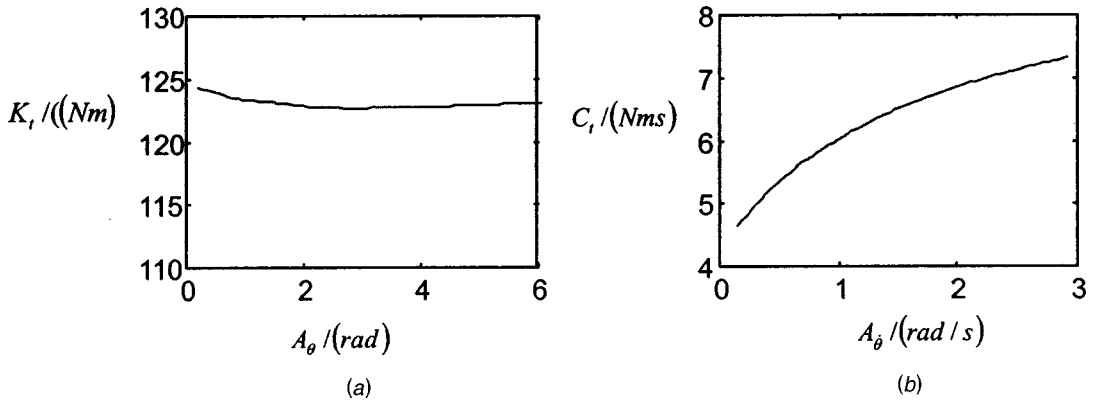

Fig. 7 The dynamic parameters versus the amplitude of response

nique proposed in references [3,4]. In such instances, the result obtained by the narrow-band filtering technique may be far from the accurate value.

Example 2. Consider the following system

$$\ddot{y}+c\dot{y}+M\cdot sign(\dot{y})+F(y)=0 \tag{47}$$

where $F(y)$ is the elastic force of a bilinear spring

$$F(y)=\begin{cases} k_1 y & |y|\leqslant y_0 \\ k_2 y+sign(y)(k_1-k_2)y_0 & |y|>y_0 \end{cases}$$

The system is with viscous damping and dry friction. The parameters are

$$k_1=900\pi^2, \quad k_2=7300\pi^2, \quad y_0=0.5$$

$$c=0.3\pi, \quad M=5\pi$$

The frequency skeleton curve and damping skeleton curve are

$$\omega_0(a)=\begin{cases} \left[k_2+\dfrac{2(k_1-k_2)}{\pi}\left(\sin^{-1}\left(\dfrac{y_0}{a}\right)+\dfrac{y_0}{a}\sqrt{1-\dfrac{y_0^2}{a^2}}\right)\right]^{1/2} & a\geqslant y_0 \\ \sqrt{k_1} & a<y_0 \end{cases} \tag{48}$$

$$h_0(a\omega)=\frac{c}{2}+\frac{2}{\pi}M\cdot[a\omega]^{-1} \tag{49}$$

We use the free vibration response with the following initial condition.

$$y(0)=15, \quad \dot{y}(0)=0, \quad \ddot{y}(0)=0$$

The instantaneous frequency of the displacement signal versus time can be seen in Fig. 3. Although this system is with a high level of nonlinearity in the common point of view, the response is almost an asymptotic signal. So the method proposed in this paper may be applied to this system. The skeleton curves identified are shown in Fig. 4.

From the preceding examples we could see that the result identified though the approach developed in this paper is in good agreement with the theoretical value.

Example 3. The dynamic characteristic of a type of torsion damper is studied through the SLM and the time-frequency filtering technique in this section. The cross section of the damper is shown as Fig. 5. The interior of the damper is filled with silicon oil. The parameters are listed in Table 1, where J denotes the moment of inertia. l denotes length of the beam. K denotes the equivalent stiffness coefficient of the spring, M is a lumped mass.

The testing system is shown as Fig. 6. It can be described by the following S.D.O.F. system

$$(J+Ml_2^2)\ddot{\theta}+C_t\dot{\theta}+[Kl_1^2+K_t]\theta=F(t)l_3 \tag{50}$$

where K_t and C_t are the torsion stiffness coefficient and torsion damping coefficient provided by the damper.

The corresponding skeleton linear model is:

$$\ddot{\theta}+2h_0(A_{\dot{\theta}})\dot{\theta}+\omega_0^2(A_\theta)\theta=\frac{1}{M_e}F(t)l_3 \tag{51}$$

where $M_e=J+Ml_2^2$. A_0 and $A_{\dot{\theta}}$ are the instantaneous amplitude of $\theta(t)$ and $\dot{\theta}(t)$.

The impulse response data is used for the identification. An acceleration sensor is placed on the lumped mass M. The principal component $\ddot{y}(t)$ is extracted from the measured acceleration signal. $\dot{y}$ and y are obtained from the integral procedure. Within a small displacement, there is

$$\theta(t)\approx\frac{y(t)}{l_2}, \quad \dot{\theta}(t)\approx\frac{\dot{y}(t)}{l_2}, \quad \ddot{\theta}(t)\approx\frac{\ddot{y}(t)}{l_2}$$

We get $h_0(t)$ and $\omega_0(t)$ by substituting $\theta(t)$, $\dot{\theta}(t)$, $\ddot{\theta}(t)$ into Eqs. (18) and (19). Then the torsion stiffness and torsion damping of the damper can be calculated as follows:

$$C_t(t)=2M_e h_0(t)=1.6887h_0(t) \tag{52}$$

$$K_t(t)=M_e\omega_0^2(t)-Kl_1^2=0.8443\omega_0^2(t)-246.9240 \tag{53}$$

The curve of $K_t(t)$ versus $A_\theta(t)$, together with that of $C_t(t)$ versus $A_{\dot{\theta}}(t)$ are plotted at each moment in Fig. 7. From them we could see the dynamic characteristic of the damper. Figure 7(*a*) shows that the torsion stiffness coefficient decreases with $A_\theta(t)$ when $A_\theta(t)$ is less than 2 radian. Within $A_\theta=2\sim6$ radian the torsion stiffness may be taken as linear because K_t is almost a constant. And Fig. 7(*b*) shows that the torsion damping increases with the amplitude of the rotation velocity. The nonlinearity in the torsion damping is rather high.

5 Conclusions

In general, the behavior of nonlinear systems varies with its instantaneous response. The nonlinearity is studied quantitatively based on the nonstationary vibration response by using the time-frequency filtering method in this paper.

In the previous paper [1] of our work, based on the quadratic time-frequency distribution of Cohen class, the skeleton linear model (SLM) and skeleton curves are constructed for a class of nonlinear system. Characteristics of the stiffness and damping of the nonlinear system may be described quantificationally with them.

In this paper the identification procedure of the skeleton curves is studied through the time-frequency filtering technique. Two time-frequency filtering methods are discussed. One is based on the quadratic time-frequency distribution and its inverse transform, the other is based on the quadratic time-frequency distribution and the wavelet transform. Both numerical examples and an experimental application are given to illustrate the validity of the technique.

By comparison with other methods, the method developed here appears very interesting in regard to precision, formulation, testing work, and computational time. The numerical results are in good agreement with theoretical predictions. Further study is expected in the future.

References

[1] Wang, L., Zhang, J., Wang, C., and Hu, S., "Time-Frequency Analysis of Non-linear Systems: the Skeleton Linear Model and the Skeleton Curves," ASME J. Vibr. Acoust., to be published.

[2] Cohen, L., 1995, *Time-Frequency Analysis: Theory and Applications*, Prentice Hall.

[3] Feldman, M., 1994, "Non-linear System Vibration Analysis Using Hilbert Transform, I. Free Vibration Analysis Method 'Freevib'," Mech. Syst. Signal Process., **8**(2), pp. 119–127.

[4] Feldman, M., 1994, "Non-linear System Vibration Analysis Using Hilbert Transform, II. Forced Vibration Analysis Method 'Forcevib'," Mech. Syst. Signal Process., **8**(3), pp. 309–318.

[5] Delprat, N., Escudie, B., Guillemain, P., et al., 1992, "Asymptotic Wavelet and Gabor Analysis: Extraction of Instantaneous Frequencies," IEEE Trans. Inf. Theory, **38**(2), pp. 644–664.

[6] Grossmann, A., Morlet, J., and Paul, T., 1985, "Transforms Associated to Square Integrable Group Representations, I: General results," J. Math. Phys., **26**(10), pp. 2473–2479.